

Numerical Study of Electromagnetic Waves Generated by a Prototype Dielectric Logging Tool

Karl J. Ellefsen*, Jared D. Abraham*, David L. Wright*, and Aldo T. Mazzella*

*U.S. Geological Survey, MS 964, Box 25046, Denver, Colorado 80225-0046, Email:
ellefsen@usgs.gov, jdabrahs@usgs.gov, dwright@usgs.gov

:U.S. EPA, PO Box 93478, Las Vegas, Nevada 89193-3478, Email:
mazzella.aldo@epa.gov

ABSTRACT

To understand the electromagnetic waves generated by a prototype dielectric logging tool, a numerical study was conducted using both the finite-difference, time-domain method and a frequency-wave number method. When the propagation velocity in the borehole was greater than that in the formation (e.g., an air-filled borehole in the unsaturated zone), only a guided wave propagated along the borehole. As the frequency decreased, both the phase and the group velocities of the guided wave asymptotically approached the phase velocity of a plane wave in the formation. The guided wave radiated electromagnetic energy into the formation, causing its amplitude to decrease. When the propagation velocity in the borehole was less than that in the formation (e.g., a water-filled borehole in the saturated zone), both a refracted wave and a guided wave propagated along the borehole. The velocity of the refracted wave equaled the phase velocity of a plane wave in the formation, and the refracted wave preceded the guided wave. As the frequency decreased, both the phase and the group velocities of the guided wave asymptotically approached the phase velocity of a plane wave in the formation. The guided wave did not radiate electromagnetic

energy into the formation. To analyze traces recorded by the prototype tool during laboratory tests, they were compared to traces calculated with the finite difference method. The first parts of both the recorded and the calculated traces were similar, indicating that guided and refracted waves indeed propagated along the prototype tool.

INTRODUCTION □

For many investigations of the near-surface, measurements of dielectric permittivity may be helpful. There are several reasons why. First, for some investigations, ground penetrating radar is used to characterize heterogeneity near the ground surface (Davis and Annan, 1989) and crosswell radar is used to characterize heterogeneity between wells (Olsson et al., 1992). For both methods, the processing and the interpretation of the data may be improved with independent measurements of the dielectric permittivity, because this property strongly affects the velocity of the radar waves. Second, many hydrological investigations require measurements of porosity because it affects the flow of groundwater and contaminants. In the saturated zone, porosity may be inferred from dielectric permittivity because the water in the pores strongly affects the permittivity (Arulanandan, 1991). Third, ground water is sometimes contaminated by dense or light non-aqueous phase liquids (MacDonald and Kavanaugh, 1994). Monitoring the cleanup of these contaminants may be possible using measurements of the permittivity because the relative permittivity of these contaminants is about 3 or 4, whereas that of water is about 80 (Greenhouse et al., 1993).

To measure dielectric permittivity in situ for a near-surface investigation, a prototype dielectric logging tool was built (Abraham, 1999). This tool is especially suitable for near-surface investigations. Its diameter is about 4.7 cm so that it can operate in small-diameter boreholes. Because the tool is easily taken apart and consists of only a few parts, the tool can be easily cleaned, a feature that is helpful when logging in contaminated wells. To operate this tool, a voltage pulse is applied to a radial waveguide, generating primarily a transverse magnetic (TM) wave. (In a cylindrical coordinate system with its z-axis aligned with the borehole, a TM wave has only one component of the magnetic field, and it is in the azimuthal

direction.) The TM wave propagates out of the radial waveguide and along the borehole, and it is detected by another radial waveguide.

To interpret the data from the prototype tool, a geophysicist must understand how the electromagnetic wave is affected by the borehole geometry (e.g., the radius) and by the electromagnetic properties of the borehole fluid and the formation. To this end, the tool was tested in a laboratory because the conditions here could be carefully controlled (Abraham, 1999 and 2000). These tests were conducted in a tank that was filled with various materials like dry sand, wet sand, and water; in the center of the tank was a borehole that contained the tool. The tests showed that both the traveltimes and the amplitude of the recorded wave were affected by the borehole radius and by the dielectric permittivities of the formation and the borehole fluid. Furthermore, the wave was affected by thin sedimentary beds in the formation. For the various formations, the traveltimes of the wave were used to estimate their dielectric permittivities, but these estimates differed significantly from independently measured values. Consequently, Abraham (1999) believed that the electromagnetic wave propagated as a guided wave, and he recommended that wave propagation be studied using numerical simulation.

Within the oil industry, many different dielectric logging tools have been developed, but almost all tools are based on two different designs (Shen, 1985; Wright and Nelson, 1993). One design uses a coil to generate a transverse electric wave that is at a single frequency, usually between 20 and 60 MHz (Hearst et al., 2000, 137-138). (In a cylindrical coordinate system with its z-axis aligned with the borehole, a transverse electric wave has only one component of the electric field, and it is in the azimuthal direction.) The other design has an array of aperture antennas (Balanis, 1997, 584-603) mounted on a metallic pad that is pushed against the borehole wall. The aperture antennas operate as either transmitters or receivers, which generate or detect a wave at a single frequency, usually about 1 GHz (Hearst et al., 2000, 138). Because both designs of the industry tools differ substantially from the prototype tool, the numerous analyses of the industry tools are not helpful in understanding the prototype tool (Freedman and Vogiatzis, 1979; Chew and Gianzero, 1981; Anderson and Chang, 1983; Chew et al., 1984; Chew and Anderson, 1985; Safinya et al., 1985, Chew, 1988; Anderson and Chew, 1989).

The goal of this study is to obtain some insight into the electromagnetic waves generated by the prototype dielectric logging tool. The study is conducted with two different types of numerical simulations. One type, which is in the time domain, uses the finite difference method to calculate both traces and snapshots of the propagating electromagnetic waves. (In this article, a trace is defined as a graph of a time-varying voltage or electric field and is analogous to a seismic trace.) The other type, which is in the frequency domain, is used to calculate the phase velocity, the group velocity, and the attenuation coefficient of the wave propagating along the borehole. The results of the numerical study show how the formation and the borehole affect the electromagnetic waves. To understand better the data recorded by the prototype tool during the laboratory tests, the tests are simulated with the finite difference method.

DIELECTRIC LOGGING TOOL

The prototype dielectric logging tool is housed inside a cylindrical fiberglass tube that has brass caps at the top and the bottom (Figure 1a); this housing prevents water and liquid contaminants from contacting the tool. The length of the fiberglass tube is 122 cm, and thickness of the tube-wall is 1.3 mm. The top brass cap attaches to a cablehead, where coaxial cables within the tool attach to coaxial cables within the logging cable.

The tool includes a radial waveguide that generates an electromagnetic wave (Figures 1b and 1c). This waveguide is called the “transmitter,” and its abbreviation is “TX.” The tool includes another radial waveguide that detects the electromagnetic wave. This waveguide is called the “receiver,” and its abbreviation is “RX.” Between the transmitter and the receiver is metal tubing having three different lengths so that there may be three different distances between the transmitter and the receiver: 7.6, 15.2, and 30.5 cm. (These distances are measured from the midpoints of the transmitter and the receiver.) Both the tubing above the transmitter and the tubing below the receiver are 39.4 cm long. The outer diameter of the tool is 4.2 cm.

The transmitter (Figure 1c) consists of two metal disks and a plastic ring, which keeps the two disks apart and parallel. Attached to the center of the top disk is a coaxial cable, which is called the “TX coaxial cable.” Near the center of the top disk is another coaxial cable, which is used to monitor the voltage in the transmitter. Like the transmitter, the receiver consists of two metal disks and a plastic ring. Attached to the center of the bottom disk is a coaxial cable, which is called the “RX coaxial cable.” This cable passes through holes in the receiver and the transmitter. All three coaxial cables have a characteristic impedance of 50 Ω . Additional information about the dimensions of the dielectric logging tool are in Abraham (1999, 53-61, 185-188).

When collecting logging data, a voltage pulse is generated by electronic equipment that is at the ground surface, and the pulse is conducted along a coaxial cable within the logging cable and then along the TX coaxial cable within the tool. When the pulse reaches the transmitter, it generates an electromagnetic wave that propagates out of the transmitter, into the formation, and along the borehole. Part of this wave propagates into the receiver and generates a voltage pulse within the RX coaxial cable. This pulse is conducted along the RX coaxial cable within the tool and then along another coaxial cable within the logging cable. At the ground surface, this pulse is digitized by electronic equipment. Each digital sample has 16 bits, The sample interval is 10 ps, and the duration each trace is 25 ns. To minimize random noise, 16 traces are stacked to form one trace.

NUMERICAL STUDY

Introductory remarks

The numerical study is conducted using two different, but complementary methods. The first is the finite-difference, time-domain (FDTD) method, which simulates the propagation of electromagnetic waves using a grid. An advantage of this method is that wave propagation is easily simulated in heterogeneous models, including models with coaxial cables and antennas. Another advantage is that the waves propagating within the model can be viewed, and so the effects of the model on the waves can be readily

discerned. The second method is formulated in the frequency-wavenumber domain **and** is called the “FK method” in this article. An advantage of this method is that it can readily calculate the properties of a guided wave over a wide range of frequencies.

FDTD method

The dielectric logging tool is a type of antenna. Simulating antennas using the FDTD method is completely described in Kunz and Luebbers (1993,263-297), Taflove (1995,475-510), and Stutzman and Thiele (1998, 493-544), and consequently only a few remarks are necessary. This implementation of the FDTD method is formulated in circular cylindrical coordinates with the z-axis aligned with the borehole axis. The entire model - the formation, the borehole, and the tool - is symmetric about the z-axis. Because of this symmetry, the computations are performed in only the r and z directions (Kunz and Luebbers, 1993,383-386), greatly reducing the amount of computation. Electromagnetic waves are introduced into the model using a coaxial cable, and the techniques for simulating wave propagation in these cables is described in Maloney (1992, 32-35).

To minimize numerical dispersion, which is inherent to the FDTD method, the spacing between the grid points is chosen so that, far away from the tool, there are at least 10 grid points for the smallest wavelength. Near the tool, however, the electromagnetic field changes rapidly. To minimize numerical dispersion here, there are at least 50 grid points for the smallest wavelength. Thus, the grid density changes within the model, and the implementation of this type of grid is described by Taflove (1995, 344-353). The edges of the grid (except that edge along the borehole axis) are absorbing boundaries (Taflove, 1995, 158-160), which simulate a grid extending to infinity. Thus, waves impinging on the absorbing boundaries have practically no reflection. This implementation of the FDTD method was tested by simulating the electromagnetic waves radiated by laboratory-scale antennas built and analyzed by Maloney (1992, 156-173). The calculated traces were practically identical to those measured by Maloney (1992, 229-253), indicating that this FDTD implementation is both accurate and correct. The computer code for this FDTD implementation is available via the internet (Ellefsen, 2002).

The model used for the FDTD simulations is pictured in Figure 2; its electromagnetic properties and dimensions are listed in Table 1. The model consists of a tool in a borehole through a homogenous formation. The tool itself consists of two solid metallic cylinders, a transmitter, and a TX coaxial cable. Each solid metallic cylinder represents a metal tube in the prototype tool. The features in the model and the corresponding features in the prototype tool have practically identical dimensions and electromagnetic properties.

The model tool omits several complex features of the prototype tool: the plastic ring in the transmitter, the TX coaxial cable for monitoring, the receiver, the RX coaxial cable, the fiberglass sheath, the top and bottoms caps, the cablehead, and the logging cable. Thus, the model tool is a simplification of the prototype tool. Nonetheless, the model tool still represents many important features of the prototype tool, and so the FDTD simulations can be used to learn the general behavior of the electromagnetic waves. Many of the aforementioned complex features are added to the model that is used to analyze the laboratory data.

Within the TX coaxial cable, the applied voltage V is a Gaussian function:

$$V(t) = s \exp\left\{-\frac{1}{4} [2\pi f_0(t - t_s)]^2\right\} \quad (1)$$

where s is a scaling factor, f_0 is frequency, t is time, and t_s is a time shift. For these simulations, $s=8.9$ V, $f_0=700$ MHz, and $t_s=1.6$ ns. This applied voltage and its frequency spectrum are plotted in Figure 3. The duration of the applied voltage is about 2 ns, and its peak amplitude is 8.9 V. In the frequency domain, the amplitudes are significant between 0 Hz and about 1.4 GHz.

FK method

The model used for the FK simulations is pictured in Figure 4; its electromagnetic properties and dimensions are listed in Table 1. The model consists of a metal cylinder in a borehole through a homogeneous formation; the metal cylinder simulates the metal tubing in the prototype tool. Locations in

the model are specified with a circular cylindrical coordinate system whose z-axis is aligned with the center of the borehole. The model extends to infinity in both the r and the z directions. The model omits features of the prototype tool like the transmitter, the receiver, and the ends of the tubing. Thus, the model is most suited to analyzing the waves propagating along the borehole, far away from these omitted features.

Wave propagation in this model is characterized by a single equation that is derived from analytical expressions for the electromagnetic field (Appendix) This equation is solved for k_z , the complex wavenumber along the z-axis. In the analytical expressions for the waves, propagation along the z-axis is described by the term $\exp(i k_z z)$, which equals $\exp(i \operatorname{Re} k_z z) \exp(-\operatorname{Im} k_z z)$. The first exponential describes the change in the wave's phase in the z direction; the factor $\operatorname{Re} k_z$ is used to calculate the phase velocity with the formula $w / \operatorname{Re} k_z$, where w is the angular frequency. From $\operatorname{Re} k_z$, the group velocity is calculated with the formula $dw/d(\operatorname{Re} k_z)$ (Stratton, 1941, 330-333). The second exponential describes the decrease in the wave's amplitude in the z direction; the factor $\operatorname{Im} k_z$ is usually called the attenuation coefficient. Thus, from the FK simulations, the phase velocity, the group velocity, and the attenuation coefficient are calculated as functions of frequency.

While many geophysicists are familiar with the concepts of phase velocity, group velocity, and dispersion, a few definitions may be helpful. Phase velocity is defined as the velocity at which a surface of constant phase (of the electromagnetic field) propagates. Group velocity is defined as the velocity at which wave packets propagate. Usually, the group velocity equals the velocity of energy propagation, which is the velocity at which the electromagnetic energy travels. However, there are exceptions, and one is encountered in this numerical study. Dispersion is defined as the spreading of a wave packet because its phase velocity is a function of frequency. Thorough discussions of phase velocity, group velocity, and dispersion are in Brillouin (1960, 17-137) and Stratton (1941, 321-340).

Dry model

The first set of simulations is for a dry model in which the borehole contains air and the formation contains dry sand. The electromagnetic properties of the air and the dry sand are listed in Table I, For both the air and the dry sand, the electrical conductivity is 0 S/m, the dielectric permittivity is independent of frequency, and the magnetic permeability is independent of frequency. These particular properties are used because they do not cause dispersion and attenuation, which would complicate the analysis of the waves.

During the FDTD simulation, the radial component of the electric field (&) is recorded everywhere on the FDTD grid. From this, snapshots of the field are made, and eight are shown in Figure 5. At 1.25 ns, the electric field has just started to radiate from the transmitter into the borehole and the formation. This radiation continues for the duration of the applied voltage pulse, about 2 ns. By about 4.25 ns, the electric field shows four distinct parts: (1) Near the transmitter is a non-propagating field that is caused by charges both within the transmitter itself and on the side of the metal cylinder (see e.g., Maloney et al., 1990). As time increases, these charges gradually migrate into the TX coaxial cable, and the non-propagating field diminishes. (2) Within both the borehole and the formation is a high amplitude wave, which is called a “guided wave” because its propagation is guided along the borehole. The electromagnetic field associated with the guided wave is not confined to the borehole the field extends into the formation and is observable up to a radial distance of about 0.5 m. Beyond this distance, the amplitude of the field is small. Because the guided wave or propagates in both the borehole and the formation, both affect its behavior. (3) Closely associated with the guided wave is a linear wavefront that is only in the formation. As the guided wave propagates along the borehole, it radiates energy into the formation -the guided wave acts essentially as a moving source. The radiated energy constructively and destructively interferes, forming the linear wavefront. Similar linear wavefronts are also generated under certain conditions during acoustic logging (deBruin and Huizer, 1989; Meredith et al., 1993) and the rupture of faults (Ben-Menahem and Singh, 1987). (4) In the formation is a spherical wavefront that propagates outward from the transmitter. Its velocity is about 1.7×10^8 m/s, which equals the velocity of a plane wave in the dry sand.

Of the four parts of the electric field that are apparent in the snapshot at 4.25 ns (Figure 5), the most important is the guided wave because only it would be detected by the receiver in the prototype tool. To analyze the guided wave, traces of E_r are recorded alongside the metal cylinder, inside the borehole (Figure 6). The maximum amplitude of the trace at 30 cm is about 234 V/m, and the maximum of the trace at 75 cm is about 170 V/m. This decrease is not caused by the electromagnetic properties of the air or dry sand; rather, it is caused primarily by the radiation of energy from the borehole into the formation. Another, less important cause is the change in the constructive interference of different frequency components that propagate at different phase velocities, a point that is discussed later. The duration of the pulse is about 2.7 ns for the trace at 30 cm and increases to about 3.2 ns for the trace at 75 cm. This increase indicates that dispersion is occurring. This dispersion is not caused by the electromagnetic properties of the air or the dry sand; rather, it is inherent to the guided wave. From the traveltimes, the velocity is calculated to be about 2.0×10^8 m/s, which is between the velocities of a plane wave in dry sand (1.7×10^8 m/s) and a plane wave in air (3.0×10^8 m/s). These observations are explained later in more detail using the results of the FK simulation.

A FK simulation of the guided wave in the dry model is used to calculate the attenuation coefficient, the phase velocity, and the group velocity between 10 MHz and 10 GHz (Figure 7). The attenuation coefficient is merely 2.7×10^{-3} neper/m at 10 MHz and increases gradually to 45 neper/m at 10 GHz. The reason for the non-zero attenuation coefficient is that the guided wave radiates energy into the formation; the increase in the attenuation coefficient with frequency indicates that the radiation increases with frequency. Below about 2 GHz, the phase and the group velocities of the guided wave asymptotically approach the phase velocity of a plane wave in dry sand. In contrast, above about 8 GHz, the phase and the group velocities of the guided wave asymptotically approach the phase velocity of a plane wave in air. Thus, the guided wave is strongly affected by the electromagnetic properties of the formation below 2 GHz, by the properties of the borehole above 8 GHz, and by both between 2 and 8 GHz. The group velocity always exceeds the phase velocity, a property called “anomalous dispersion” (Stratton, 1941, 340). Above about 2.4 GHz, the group velocity of the guided wave exceeds 3×10^8 m/s, which is the speed of light in a vacuum, While this phenomenon appears to violate a law of physics, it does not; Stratton (1941, 333-340)

and Brillouin (1960, 85-111) explain this phenomenon for plane waves. As a practical matter, the phenomenon is unimportant because, at 2.4 GHz, the attenuation coefficient is 20 neper/m, indicating that, at this frequency and higher frequencies, the guided wave propagates only a short distance from the transmitter.

The traces in Figure 6 are about one-fifth of all traces recorded in the borehole during the FDTD simulation. This large set of traces is processed with a two-dimensional spectral estimation technique (Ellefsen et al., 1989), which estimates the attenuation coefficient, the phase velocity, and the amplitude at each frequency (black dots in Figure 7). The interval between the estimates is 93 MHz, and the first estimate is at 93 MHz. The estimated attenuation coefficients are somewhat close to the coefficients calculated with the FK method. The discrepancy is caused entirely by the difficulty in estimating these coefficients (Ellefsen et al., 1989). The estimated phase velocities are close to the phase velocities calculated with the FK method. The estimated amplitudes are large between 93 MHz and about 1 GHz; they decrease markedly thereafter and are practically insignificant at 2.1 GHz. Thus, practically all information in the traces is in the frequencies between 93 MHz and 2.1 GHz.

Between 93 MHz and 2.1 GHz, the calculated attenuation coefficient ranges from 0.058 to 15 neper/m; these non-zero attenuation coefficients quantify the decrease in the amplitude of the traces (Figure 6). Between 93 MHz and 2.1 GHz, the calculated group velocity ranges from 1.82×10^8 to 2.53×10^8 m/s. This increase in the group velocity causes the broadening of the pulse observed in the traces. In addition, this range of group velocities brackets the velocity estimated from the traveltimes of the traces (2×10^8 m/s). While it would seem that the velocity estimated from the traveltimes should be close to 2.53×10^8 m/s, group velocities that are greater than about 2×10^8 m/s are associated with high attenuation coefficients and low amplitudes, making these frequency components difficult to observe in the traces.

Wet model

The second set of simulations is for a wet model in which the borehole contains water and the formation contains wet sand. The electromagnetic properties of the water and the wet sand are listed in Table 1. For both the water and the wet sand, the electrical conductivity is 0 S/m, the dielectric permittivity is independent of frequency, and the magnetic permeability is independent of frequency. These particular electromagnetic properties do not cause dispersion and attenuation.

Eight snapshots of the electric field (E_r) are shown in Figure 8. At 2.5 ns, the field has just started to radiate from the transmitter into the borehole and the formation. This radiation continues for the duration of the applied voltage pulse, about 2 ns. By about 7.5 ns, the electric field shows three distinct parts:

- (1) Near the transmitter is a non-propagating field that is caused by charges within the transmitter and along the metal cylinder. The charges migrate into the coaxial cable, and the non-propagating field diminishes with time.
- (2) In the formation is a spherical wavefront, and its propagation velocity is about 0.75×10^8 m/s, which equals the velocity of a plane wave in the wet sand. Although the spherical wavefront appears to be missing between about 85° and 95° (measured from the borehole axis), the wavefront is not missing - the amplitude of E_r is just very small.
- (3) Within both the borehole and in the formation is a guided wave. In addition to these three distinct parts of the electric field, there is also a refracted wave in the borehole, which cannot be observed in these snapshots because of their scale. However, a close-up snapshot of the field shows this refracted wave (Figure 9). The refracted wave propagates from the formation into the borehole, and it precedes the guided wave.

Traces of E_r that are recorded inside the borehole are shown in Figure 10. Although the traces show both the refracted and the guided waves, the two waves are not distinct because their velocities are similar. This point is discussed later. The duration of the waves is about 6.9 ns for the trace at 30 cm and increases to about 15.4 ns for the trace at 75 cm. This increase indicates that dispersion is occurring. This dispersion is not caused by the electromagnetic properties of the water and the wet sand; rather, this dispersion is an inherent property of the guided wave. The amplitude is about 9.1 V/m for the trace at

30 cm and about 7.7 V/m for the trace at 75 cm. This decrease is not caused by intrinsic attenuation in the water and the wet sand; rather the decrease is caused by the dispersion of the guided wave, which changes the constructive interference of different frequency components. From the traveltimes, which are measured at the onset of the refracted wave, the velocity is calculated to be about 0.74×10^8 m/s; the error in the calculated velocity caused by errors in the traveltimes is estimated to be about 0.05×10^8 m/s. Thus, the calculated velocity equals, within the margin of error, the velocity of a plane wave in wet sand, which is 0.75×10^8 m/s. □

The attenuation coefficient, the phase velocity, and the group velocity (Figure 11) are calculated with a FK simulation for the guided wave, but not the refracted wave. At all frequencies, the calculated attenuation coefficient is 0 neper/m because the electromagnetic properties themselves do not cause attenuation, and energy is not radiated into the formation. Below about 300 MHz, the calculated phase and group velocities asymptotically approach the phase velocity of a plane wave in wet sand. Above about 3 GHz, the calculated phase and group velocities asymptotically approach the phase velocity of a plane wave in water. Thus, the guided wave is strongly affected by the electromagnetic properties of the formation below 300 MHz, by the properties of the borehole above 3 GHz, and by both between 300 MHz and 3 GHz. The group velocity is always less than the phase velocity, a phenomenon called “normal dispersion” (Stratton, 1941, 340).

The traces are processed with the two-dimensional spectral estimation technique (Ellefsen et al., 1989) to estimate the attenuation coefficient, the phase velocity, and the amplitude for the guided wave (Figure 1). The interval between the estimates is 33 MHz, and the first estimate is at 33 MHz. The estimated attenuation coefficients are somewhat close to the coefficients calculated with the FK simulation; the discrepancy is caused entirely by the difficulty of estimating these coefficients. The estimated phase velocities are very close to the calculated phase velocities. The estimated amplitudes are large between 33 MHz and about 1.3 GHz; they decrease markedly thereafter and are practically insignificant at 2.4 GHz. Thus, in the traces, all information about the guided wave is in the frequencies between 33 MHz and 2.4 GHz.

Below about 300 MHz, the group velocity of the guided wave is about 0.73×10^8 m/s (Figure 11 b), which is very close to the velocity of the refracted wave, $0.75 \sim 10^8$ m/s. Consequently, in the traces (Figure 10), the low frequency components of the guided wave overlap the refracted wave - the two waves are not separate. The group velocity of the guided wave decreases from 0.73×10^8 m/s at 33 MHz to 0.29×10^8 m/s at 2.4 GHz (Figure 11 b). In other words, the high frequency components propagate much slower than the low frequency components propagate. This difference causes the ringing in the traces and the duration of the guided wave to increase as the distance from the transmitter increases (Figure 10). Because the high frequency components of the guided wave have low amplitudes (Figure 11c), the ringing in the traces has low amplitude (Figure 10).

ANALYSIS OF LABORATORY DATA

Laboratory tests

The laboratory tests of the prototype dielectric logging tool were conducted in a plastic, cylindrical tank that was 1.20 m high and 0.70 m in diameter. In the center of the tank was a plastic pipe that functioned as borehole casing. The tank was filled with various materials that, in a field setting, would represent the formation. Although Abraham (1999,71-77, 194-215) tested the tool with many different combinations of materials for the borehole and the formation, only two combinations are considered here. For the “dry laboratory model,” the borehole contained air, and the formation contained dry sand. For the “wet laboratory model,” the borehole contained water, and the formation contained wet sand.

The water used for the wet laboratory model was deionized, and its measured electrical conductivity was 1.0×10^{-6} S/m (Abraham, 1999, 78). The sand used for both formations was silica sand with a porosity of 44%. The electromagnetic properties of both formations were measured in the laboratory (Abraham, 1999, 77-79). using the procedures described in Canan (1999,70-86). The measured properties are listed in Table 2. For both formations, the real part of the relative dielectric permittivity and the real part

of the relative magnetic permeability were practically independent of frequency. The electromagnetic properties that attenuate a wave (i.e., electrical conductivity, the imaginary part of the dielectric permittivity, and the imaginary part of the magnetic permeability) were measured collectively as the loss tangent (Balanis, 1989, 78-79). For the dry sand, the loss tangent was below the detection limit of the measuring equipment.

The voltage applied to the transmitter was measured directly by connecting the TX coaxial cable to an oscilloscope. The applied voltage (Figure 12a) rose from about 0 to 9 V within about 1 ns; thereafter, the voltage decayed gradually. In the frequency domain (Figure 12b), the amplitudes were significant between 0 and about 1.7 GHz. During the laboratory tests, the voltage pulse from the receiver propagated along the RX coaxial cable, through the cable head, and then along another coaxial cable that was inside the logging cable. The effects of this propagation were measured and then represented mathematically by a transfer function (Lathi, 1965, 26-28). An inverse of the transfer function was applied to all traces, and so the traces in Figure 13 effectively show the voltage in the RX coaxial cable where it attaches to the receiver.

FDTD simulations □

The traces from the laboratory tests are analyzed using FDTD simulations. The model for the simulations is identical to that used in the numerical study (Figure 2 and Table 1), with two exceptions. First, the model includes a receiver, whose structure is identical to that of the transmitter in Figure 2b. Between the receiver and the transmitter is a metal cylinder with three different lengths, because there are three different lengths of metal tubing between the transmitter and the receiver in the prototype tool. Second, the model includes plastic casing just like the plastic pipe used in the laboratory tests, includes a fiberglass sheath just like the prototype tool, and includes plastic rings within the transmitter and the receiver just like the prototype tool. The electromagnetic properties and dimensions of the model features associated with these two exceptions are listed in Table 3. Including these features in the model makes it a reasonable representation of both the prototype tool and the tank, which were used in the laboratory tests.

When the formation in the model is dry sand, its electromagnetic properties (Table 3) are identical to the measured properties of dry sand (Table 2). However, when the formation in the model is wet sand, its relative permittivity is slightly lower than the measured value. The reason for using the different value is that it improves the match between the calculated and the measured traces. This difference in the permittivities may be caused by a difference in the water saturation. The measured sample of wet sand was probably completely saturated with water, whereas the wet sand in the tank may have had a small amount of air trapped in some isolated pores. Such trapped air is difficult to remove, and its effect is to lower the relative permittivity. Also, when the formation in the model is wet sand, its electromagnetic properties (Table 3) do not account for the modest loss tangent (Table 2).

While the applied voltage (Figure 12a) could be used directly in the FDTD simulations, this is somewhat inconvenient because its sample interval differs from the time step for the FDTD simulation. Instead, the applied voltage is approximated by an analytical function, which is a modification of a function in Lathi (1965, 136). The analytical function is

$$V(t) = s(t - t_s)^a \exp\left\{-\frac{(t - t_s)}{\gamma}\right\} u(t - t_s) \quad (2)$$

where s is a scaling factor, t is time, t_s is a time shift, a is a dimensionless exponent, γ is a coefficient (with a dimension of time), and u is the Heaviside step function. The parameters in equation 2 are selected by fitting this analytical approximation to the measured voltage, using trial and error. The parameters giving the best fit are $s = 2.55 \times 10^{10}$, $t_s = 0.01$ ns, $a = 1.2$, and $\gamma = 0.65$ ns. The analytical approximation and the measured voltage are practically identical (Figure 12a). Likewise, the frequency spectra of the analytical approximation and the measured voltage are practically identical between 0 and about 1.5 GHz (Figure 12b).

For each model, there are three FDTD simulations for the three different lengths of tubing between the transmitter and the receiver. The three traces calculated for each model are shown in Figure 13.

Analysis of measured and calculated traces

For the dry laboratory model, compare the first events in the measured and the calculated traces (Figure 13a). For both, the amplitudes decrease as the TX-RX distance increases, their traveltimes match, and their shapes generally match. Thus, because the first event in the calculated traces is a guided wave, the first event in the measured traces is almost certainly a guided wave. A similar comparison may be made for wet laboratory model (Figure 13b), and the inference from this comparison is that first event in the measured traces is almost certainly the refracted and guided waves.

Despite the similarities in the measured and the calculated traces, there are some significant differences. For the dry laboratory model (Figure 13a), the amplitude and the duration of the guided wave are less in the measured traces than they are in the calculated traces. The measured traces show a second event that is about 4.5 ns after the guided wave. For the wet laboratory model (Figure 13b), the measured traces show a second event that is about 7 ns after the refracted and the guided waves. All of these differences are attributed to complexities in the prototype tool that are absent from the model tool.

To investigate the cause of the second event in the measured traces (Figure 13), assume that this event is a guided wave that reflects off the end of the metal tubing below the receiver (Figure 1 b). That is, this guided wave propagates past the receiver and down the metal tubing, reflects off the end of the tubing, and then propagates up the metal tubing to the receiver. The extra distance that this reflected wave propagates is twice the length of the metal tubing, **78.8 cm. (This extra distance remains the same for all TX-RX distances.)** In the dry laboratory model, the velocity of the guided wave is about 1.8×10^8 m/s. and so the expected time delay between the original and reflected waves is 4.4 ns, which is very close to that observed in the traces, 4.5 ns. Thus, the second event probably includes this reflected guided wave. Reflections may also occur from the end of the metal tubing above the transmitter (Figure 1 b), the top and bottom caps on the tool housing, and the cablehead (Figure 1 a). Thus, the second event is probably a

complex superposition of reflected guided waves. For the wet laboratory model, the second event is interpreted similarly.

The calculated traces for the wet laboratory model (Figure 13b) lack the oscillations observed in the calculated traces for the wet model in the numerical study (Figure 10). To understand this difference, recall that the traces in Figure 13b are the voltage in the RX coaxial cable where it attaches to the receiver, whereas the traces in Figure 10 are the radial component of the electric field in the annular space. In other words, the two sets of traces show different components of the field at different locations in the models. Consequently, the two sets of traces should not be expected to be identical.

DISCUSSION □

Because boreholes in the unsaturated zone are filled with air, the velocity of propagation in the borehole is higher than that in the formation. Consequently, during logging with the prototype tool, the detected electromagnetic wave is expected to be a guided wave, and its behavior is expected to be somewhat like that of the guided wave in the dry model used in the numerical study. On the other hand, boreholes in the saturated zone are filled with water, and so the velocity of propagation in the borehole is less than that in the formation. During logging, the detected electromagnetic waves are expected to be both a refracted wave and a guided wave, and their behavior is expected to be somewhat like that of the refracted and guided waves in the wet model used in the numerical study.

While the goal of this investigation is to learn about the electromagnetic waves generated by the prototype tool, not to develop methods to estimate dielectric permittivity, some speculation about suitable estimation methods is appropriate. One class of estimation methods operate in the time domain. For traces collected in the saturated zone, the traveltimes of the refracted wave would be measured. The traveltimes would be used to calculate the velocity of the refracted wave, which equals the phase velocity of a plane wave in the formation, v . Finally, v would be used to calculate the relative dielectric permittivity ϵ_r of the formation with the formula $\epsilon_r = (c/v)^2$, where c is speed of light in a vacuum (Stratton, 1941,275). The

advantages of this class of estimation methods include their simplicity and the requirement that the tool have merely two receivers. A serious disadvantage is that there is no refracted wave in the unsaturated zone, although this problem could be overcome if the borehole could be filled with water or another liquid with a high permittivity.

Another class of estimation methods operate in the frequency domain. The traces from several receivers would undergo array processing to estimate, as functions of frequency, the phase velocity and the attenuation coefficient of the guided wave (e.g., Ellefsen et al., 1989). Then, using an inversion procedure, the phase velocity and the attenuation coefficient would be used to estimate both the frequency-dependent dielectric permittivity and the electrical conductivity of the formation. An advantage of this class of estimation methods is that it provides a lot of information about the electromagnetic properties of the formation. The disadvantages include the complexity of the processing and the requirement that the tool have several receivers (i.e., more than about 6).

Before dielectric logging can be routinely used for near-surface investigations, more research and development are required of both the tool and the methods for estimating dielectric permittivity. To this end, it may be helpful to investigate propagation in models that are more representative of field conditions than the models used in this study. It may be beneficial to determine how the electromagnetic waves are affected by electrical conductivity, frequency-dependent dielectric permittivity, heterogeneity in the formation (e.g., sedimentary beds, water table), casing, casing grout, borehole radius, tool radius, and a tool that is not centered in the borehole.

CONCLUSIONS□

For both the wet and the dry models in the numerical study, the phase and the group velocities of the guided waves asymptotically approach, at low frequencies, the phase velocity of a plane wave in the formation

The low and the high frequencies at which these phenomena occur depend upon the borehole geometry and the electromagnetic properties of the borehole fluid and the formation.

In the dry model, the guided wave radiates energy into the formation, causing its amplitude to decrease especially at high frequencies. Because the group velocity of the guided wave increases only slightly with frequencies, the high and low frequency components in the traces arrive practically together. In the wet model, the behavior of the waves is very different. The guided wave does not radiate energy into the formation. Because the group velocity of the guided wave decreases with frequency, the high frequency components in the traces arrive after the low frequency components arrive. A wave is refracted from the formation into the borehole, and the velocity of this refracted wave (measured along the borehole) equals the phase velocity of a plane wave in the formation. The reason for the different behaviors in the two models is that, in the dry model, the velocity of propagation in the borehole is higher than that in the formation but, in the wet model, this relation is reversed.

To analyze the traces collected with the prototype tool during laboratory tests, they were compared with traces calculated with the FDTD method. In the dry laboratory model, the guided wave in the calculated traces corresponds to the first and largest event in the laboratory traces. Likewise, in the wet laboratory model, the guided and the refracted waves in the calculated traces correspond to the first and largest event in the laboratory traces. These findings support the hypothesis that the prototype tool detects guided and refracted waves propagating along the borehole. In addition, the analysis indicates that electromagnetic waves are probably reflected from the ends of both the tool and the tool housing.

ACKNOWLEDGMENTS AND DISCLAIMERS

The authors thank D. Fitterman, P. Nelson, two anonymous reviewers, and the associate editor for their helpful comments and suggestions. The work was funded by the Mineral Resources Program of the U.S. Geological Survey and by the U.S. Environmental Protection Agency under Interagency Agreement Number DW 14936642-0. This publication has not been subjected to the EPA's peer and administrative

review and has not been approved for publication as an EPA document. Mention of trade names or commercial products does not constitute endorsement or recommendation for use.

REFERENCES

- Arulanandan, K. 1991, Dielectric method for prediction of porosity of saturated soil: *Journal of Geotechnical Engineering* **117**, 319-330.
- Abraham, J. D., 1999, Physical modeling of a prototype slim-hole time-domain dielectric logging tool: M. SC. thesis. Colorado School of Mines.
- Abraham, J. D., 2000, Physical modeling of a prototype slim-hole time-domain dielectric logging tool: *Symposium on the Application of Geophysics to Engineering and Environmental Problems, Environmental and Engineering Geophysical Society, Proceedings*, 503-512.
- Acton, F. S., 1990, *Numerical methods that work*: Mathematical Association of America
- Anderson, B., and Chang, S K , 1983, Synthetic deep propagatinn tool response hy the finite element method: 241·Annual Logging Symposium, Sot. Prof. Well Log Analysts, Transactions, paper T.
- Anderson, B., and Chew, W. C., 1989, Transient response of some borehole mandrel tools: *Geophysics*, **54**, 216-224.
- Balanis, C. A., 1989, *Advanced engineering electromagnetics*: John Wiley & Sons, Inc
- Balanis, C. A., 1997, *Antenna theory - Analysis and design*: John Wiley & Sons, Inc.

- Ben-Menahem, A., and Singh, S. J., 1987, Supershear accelerations and Mach-waves from a rupturing front. Part I. Theoretical model and implications: *J. Phys. Earth*, **35**, 347-365.
- Brillouin, L., 1960, *Wave propagation and group velocity*: Academic Press Inc.
- Canan, B., 1999, Dielectric properties of mixtures of clay-water-organic compounds, Ph.D. thesis, Colorado School of Mines
- Chew, W. C., and Gianzero, S. C., 1981, Theoretical investigation of the electromagnetic wave propagation tool: *IEEE Trans. Geosci. Remote Sensing*, **GE-19**, 1-7.
- Chew, W. C., Barone, S., Anderson, B., Hennessy, C., 1984, Diffraction of axisymmetric waves in a borehole by bed boundary discontinuities: *Geophysics*, **49**, 1586-1595.
- Chew, W. C., and Anderson, B., 1985, Propagation of electromagnetic waves through geologic beds in a geophysical probing environment: *Radio Sci.*, **20**, 6111-621.
- Chew, W. C., 1988, Modeling of the dielectric logging tool at high frequencies -Theory: *IEEE Trans. Geosci. Remote Sensing*, **26**, 382-387.
- Davis, J. L., and Annan, A. P., 1989. Ground penetrating radar for high resolution mapping of soil and rock stratigraphy. *Geophys. Prosp.*, **37**, 53 1-551.
- deBruin, J. A. and Huizer, W., 1989, Radiation from waves in a borehole: *Scientific Drilling*, **1**, 3-10
- Ellefsen, K. J., Cheng, C. H., and Tubman, K. M., 1989, Estimating phase velocity and attenuation of guided waves in acoustic logging data: *Geophysics*, **54**, 1054-1059.

- Ellefsen, K. J., 2002, FD-BH: *A* program for simulating electromagnetic waves from a borehole antenna: U.S. Geological Survey Open-file Report 02-276. available at <http://pubs.usgs.gov/of/2002/ofr-02-0276/>.
- Freedman, R., and Vogiatzis, J. P., 1979, Theory of microwave dielectric constant logging using the electromagnetic propagation method: *Geophysics*, **44**, 969-986.
- Greenhouse, J., Brewster, M., Schneider, G., Redman, D., Annan, P., Olhoeft, G., Lucius, J., Sander, K., Mazzella, A., 1993, Geophysics and solvents: The Borden experiment: *The Leading Edge*, **12**, 261-267.
- Hearst, J. R., Nelson, P. H., and Paillet, F. L., 2000, *Well logging for physical properties-A handbook for geophysicists, geologists, and engineers*: John Wiley & Sons, Inc.
- Kunz, K. S., and Luebbers, R. J., 1993, *The finite difference time domain method for electromagnetics*: CRC Press.
- Lathi, B. P., 1965, *Signals, systems, and communication*: John Wiley & Sons, Inc.
- MacDonald, J. A., and Kavanaugh, M. C., 1994, Restoring contaminated groundwater - An achievable goal?: *Environ. Sci. and Technol.*, **28**,362-368.
- Maloney, J. G., 1992, *Analysis and synthesis of transient antennas using the finite-difference time-domain (FDTD) method*: Ph. D. thesis, Georgia Institute of Technology.
- Maloney, J. G., Smith, G. S., and Scott, W. R., Jr., 1990, Accurate computation of the radiation from simple antennas using the finite-difference time-domain method: *IEEE Transactions on Antennas and*

Meredith, J. A., Toksoz, M. N., and Cheng, C. H., 1993, Secondary shear waves from source boreholes: Geophys. Prosp., **41**,287-3 12.

Olsson, O., Falk, L., Forslund, O., Lundmark, L., and Sandberg, E., 1992, Borehole radar applied to the characterization of hydraulically conductive fracture zones in crystalline rock: Geophys. Prosp., **40**, 109-142

Safinya, K., Habashy, T., Randall, C., Clark, B., Perez-Falcon, A., 1985, Experimental and theoretical study of the electromagnetic propagation tool in layered and homogeneous media: Annual Technical Conference and Exhibition, Sot. Petr. Eng., Am. Inst. Min., Metall. Petr. Eng., Proceedings, paper SPE 14188.

Shen, L. C.. 1985, Problems in dielectric-constant logging and possible routes to their solution: The Log Analyst, **26**, 14-25.

Stratton, I. A., 1941, Electromagnetic theory McGraw-Hill Book Co.

Stutzman, W. L., and Thiele, G. A., 1998, Antenna theory and design: John Wiley & Sons, Inc.

Taflove, A., 1995, Computational electrodynamics: Artech House.

Wright, D. L., and Nelson, P. H., 1993, Borehole dielectric logging - A review and a laboratory experiment: 5th International Symposium on Geophysics for Minerals, Geotechnical, and Environmental Applications, Minerals and Geotechnical Logging Society, Proceedings, paper T.

APPENDIX

EQUATION USED FOR FK SIMULATIONS AND ITS SOLUTION

For the FK stimulations, both the phase velocity and the attenuation coefficient are calculated using an equation for electromagnetic wave propagation along a borehole. This appendix describes the derivation of this equation and a procedure for its solution.

The mathematical model consists of three concentric cylinders, which are labeled 1, 2, and 3 (Figure 4). Cylinder 1 represents the dielectric logging tool, cylinder 2 the annular space, and cylinder 3 the formation. Locations in the model are specified with a circular cylindrical coordinate system for which the z-axis is aligned with the axes of the three cylinders. The outer radii of cylinders 1, 2, and 3 are a_1 , a_2 , and a_3 , respectively. All three cylinders extend from $-\infty$ to ∞ along the z-axis. For cylinder j , the dielectric permittivity is ϵ_j , the magnetic permeability is μ_j , and the electrical conductivity is σ_j . For cylinder j , the wavenumber k_j is calculated from its electromagnetic properties via

$$k_j^2 = \mu_j \epsilon_j \omega^2 + i \mu_j \sigma_j \omega \quad (\text{A-1})$$

where ω is the frequency. This wavenumber is decomposed into two components, k_r and k_z , which are aligned with the r- and z-axes of the coordinate system. The wavenumber and its two components are related via

$$k_j^2 = k_r^2 + k_z^2 \quad (\text{A-2})$$

The component k_z is the same in all cylinders because of Snell's law (Stratton, 1941,491). The wavenumber k_j and its two components are generally complex; the real and imaginary parts of k_z , for example, are designated $\text{Re } k_z$ and $\text{Im } k_z$.

Wave propagation in this model has been extensively studied, and Stratton*^s (1941, 545-549) equation for wave propagation is used here. To derive this equation, Stratton first derived equations for symmetric TM modes in each cylinder. Then, Stratton (1941, 547) applied the boundary conditions at the interfaces between the cylinders, and the result was one equation for wave propagation in the entire model:

$$\frac{N_0(\lambda_2 a_1) - \frac{\mu_1 \lambda_1 k_2^2}{\mu_2 \lambda_2 k_1^2} \frac{J_0(\lambda_1 a_1)}{J_1(\lambda_1 a_1)} N_1(\lambda_2 a_1)}{J_0(\lambda_2 a_1) - \frac{\mu_1 \lambda_1 k_2^2}{\mu_2 \lambda_2 k_1^2} \frac{J_0(\lambda_1 a_1)}{J_1(\lambda_1 a_1)} J_1(\lambda_2 a_1)} = \frac{N_0(\lambda_2 a_2) - \frac{\mu_3 \lambda_3 k_2^2}{\mu_2 \lambda_2 k_3^2} \frac{H_0^{(1)}(\lambda_3 a_2)}{H_1^{(1)}(\lambda_3 a_2)} N_1(\lambda_2 a_2)}{J_0(\lambda_2 a_2) - \frac{\mu_3 \lambda_3 k_2^2}{\mu_2 \lambda_2 k_3^2} \frac{H_0^{(1)}(\lambda_3 a_2)}{H_1^{(1)}(\lambda_3 a_2)} J_1(\lambda_2 a_2)} \quad (\text{A-3})$$

where J_0 and J_1 are Bessel functions of the first kind, N_0 and N_1 are Bessel functions of the second kind (Neumann functions), and $H_0^{(1)}$ and $H_1^{(1)}$ are Hankel functions. Geophysicists often called equation A-3 either the dispersion equation or the period equation.

To investigate a dielectric logging tool, cylinder 1 is assigned infinite electrical conductivity, which is a suitable approximation for metal tubing. Thus, equation A-3 must be modified, and the following modification is similar to that used by Stratton (1941, 548) for investigating wave propagation in coaxial cables. As the electrical conductivity approaches infinity, equation A-1 shows that $\text{Im } k_1^*$ approaches infinity. Equation A-2 shows that, at the same time, the $\text{Im } \nu_j^2$ approaches $\text{Im } \nu_j^2$ because $\text{Im } k_j^2$ must be finite (otherwise, the wave would not propagate). Consequently, the ratio ν_j / k_j^2 approaches zero, and equation A-3 becomes

$$0 = \frac{N_0(\lambda_2 a_1)}{J_0(\lambda_2 a_1)} - \frac{N_0(\lambda_2 a_2) - \frac{\mu_3 \lambda_3 k_2^2}{\mu_2 \lambda_2 k_3^2} \frac{H_0^{(1)}(\lambda_3 a_2)}{H_1^{(1)}(\lambda_3 a_2)} N_1(\lambda_2 a_2)}{J_0(\lambda_2 a_2) - \frac{\mu_3 \lambda_3 k_2^2}{\mu_2 \lambda_2 k_3^2} \frac{H_0^{(1)}(\lambda_3 a_2)}{H_1^{(1)}(\lambda_3 a_2)} J_1(\lambda_2 a_2)} \quad (\text{A-4})$$

For this equation, variables k_2 and k_3 are calculated with equation A-1; variables β_2 in and β_3 , with equation A-2. However, equation A-2 depends upon k_2 , which is unknown. Thus, the only unknown

Because of the complexity of equation A-4, a numerical method must be used to find those k_z for which the equation is satisfied. The numerical method that is used in this investigation is a systematic search within a rectangular region of the complex plane for k_z (Figure A1). Because $\text{Re } k_z$ must be between $\text{Re } k_1$ and $\text{Re } k_3$, the equations $\text{Re } k_z = \text{Re } k_1$ and $\text{Re } k_z = \text{Re } k_3$ define two sides of the rectangular region. Because $\text{Im } k_z$ must be greater than or equal to zero, the equation $\text{Im } k_z = 0$ defines the bottom side of the rectangular region. The top side of the rectangular region depends upon the maximum value expected for $\text{Im } k_z$. For many models, a suitable maximum is about 40, and in this case, the equation $\text{Im } k_z = 40$ defines the top side of the rectangular region. Within the rectangular region, the absolute value of the right-hand-side of equation A-4 is calculated at many regularly spaced points (Figure A1). Starting from each local minimum in the absolute value, Newton's method (Acton, 1990, 51) is used to find the k_z at which the right-hand-side of equation A-4 equals zero, within a range that accounts for the finite numerical precision of the computer.

In Figures 7 and 11, the phase velocities that are calculated with this numerical method are practically identical to the phase velocities that are estimated from the traces using a two-dimensional spectral estimation technique (Ellefsen et al., 1998). The attenuation coefficients that are calculated with this numerical method are similar to the attenuation coefficients that are estimated from the traces; the differences are due entirely to difficulty of estimating these coefficients (Ellefsen et al., 1998). These results indicate that the numerical method used to solve equation A-4 is accurate.

Table 1. Electromagnetic properties and dimensions of the models used for the FDTD and FK simulations (Figures 2 and 4). Metal is represented by a perfect conductor, for which the relative dielectric permittivity and the relative magnetic permeability have no significance. Consequently, the associated table entries have leaders (---).

Item	Simulation	Material	Relative Dielectric Permittivity	Relative Magnetic Permeability	Electrical Conductivity (S/m)	Dimension (mm)
Inner conductor, TX coaxial cable	FDTD	Metal	---	---	∞	Outer radius: 0.5
Dielectric sheath, TX coaxial cable	FDTD	Plastic	1.735	1.	0.	Inner radius: 0.5 Outer radius: 1.5
Outer conductor, TX coaxial cable	FDTD	Metal	---	---	∞	Inner radius: 1.5 Outer radius: 2.0
Metal cylinder above TX	FDTD	Metal	---	---	∞	Inner radius: 2.0 Outer radius: 20.6
Metal disk above TX	FDTD	Metal	---	---	∞	Inner radius: 2.0 Outer radius: 20.6 Axial length: 5.0
Air in TX	FDTD	Air	1.	1.	0.	Inner radius: 0.5 Outer radius: 20.6 Axial length: 6.4
Metal disk below TX	FDTD	Metal	---	---	∞	Outer radius: 20.6 Axial length: 5.0
Metal cylinder below TX	FDTD	Metal	---	---	∞	Outer radius: 20.6
Metal cylinder	FK	Metal	---	---	∞	Outer radius: 20.6
Annular Space	FDTD and FK	Air or water	1. for air, 81. for water	1.	0.	Inner radius: 20.6 Outer radius: 25.4
Formation	FDTD and FK	Dry sand or wet sand	3. for dry sand, 16. for wet sand	1.	0.	Inner radius: 25.4

Table 2. Measured electromagnetic properties of the dry and the wet sands (Abraham, 1999, 78-79).

Formation	Relative Dielectric Permittivity	Relative Magnetic Permeability	Loss Tangent at 320 MHz
Dry sand	3	1	$<3.2 \times 10^{-2}$
Wet sand	18.	1.	1.0×10^{-1}

Table 3. Electromagnetic properties and dimensions of selected features of the FDTD model used to analyze the laboratory data. Selected features refer either to features not in Table 1 or to features in Table 1 whose dimensions are different. Metal is represented by a perfect conductor, for which the relative dielectric permittivity and the relative magnetic permeability have no significance. Consequently, the associated table entries have leaders (---).

Item	Material	Relative Dielectric Permittivity	Relative Magnetic Permeability	Electrical Conductivity (S/m)	Dimension (mm)
Metal cylinder between TX and RX	Metal	---	---	∞	Outer radius: 20.6 Axial lengths: 69.9, 146.1, or 298.5
Plastic rings in TX and RX	Plastic	3.6	1.	0.	Inner radius: 12.6 Outer radius: 20.6 Axial length: 6.4
Sheath	Fiberglass	4.5	1.	0.	Inner radius: 20.6 Outer radius: 21.9
Annular Space	Air or water	1. for air, 81. for water	1.	0.	Inner radius: 21.9 Outer radius: 25.4
Borehole casing	Plastic	4.	1.	0.	Inner radius: 25.4 Outer radius: 30.0
Formation	Dry sand or wet sand	3. for dry sand, 16. for wet sand	1.	0.	Inner radius: 30.0

FIG. 1. Prototype dielectric logging tool. Figures 1b and 1c show only the 7.0 cm tubing between the transmitter and the receiver. For other configurations of the tool, the 7.0 cm tubing is replaced by 14.6 cm or 29.9 cm tubing.

FIG. 2. (a) Model used for the FDTD simulations in the numerical study. This diagram is not to scale (b) Close-up view of the model near the transmitter. This diagram is to scale. The electromagnetic properties and the dimensions of the model are listed in Table 1

FIG. 3. (a) Voltage applied to the TX coaxial cable in the FDTD simulations (Figure 2). (b) Amplitude spectrum of the voltage; all amplitudes are normalized by the largest amplitude.

FIG. 4. Model used for the FK simulations in the numerical study. Variables a_1 and a_2 are the radii of the metal cylinder and the borehole, respectively. The numbers 1, 2 and 3 refer to the three regions in the model and are used in the mathematical derivation in the Appendix. The electromagnetic properties and the dimensions of the model are listed in Table 1.

FIG. 5. Snapshots from a FDTD simulation, showing wave propagation in the dry model (Figure 2). In this model, the borehole contains air, and the formation contains dry sand.

FIG. 6. Traces showing the radial component of the electric field, E_r . The traces are computed during a FDTD simulation in the dry model. The trace locations are within the borehole (black dots in Figure 5). The vertical lines correspond to the times of the snapshots (Figure 5).

FIG. 7. Attenuation coefficient, phase velocity, and group velocity of the guided wave. These quantities are calculated during a FK simulation for the dry model (Figure 4). Also shown are estimates of the attenuation coefficient, the phase velocity, and the amplitude of the guided wave, all of which are obtained by processing traces from the FDTD simulation (Figure 6).

FIG. 8. Snapshots from a FDTD simulation, showing wave propagation in the wet model (Figure 2). In this model, the borehole contains water, and the formation contains wet sand. Also see Figure 9.

FIG. 9. Snapshot from a FDTD simulation, showing the refracted wave in the wet model (Figure 2). Also see Figure 8.

FIG. 10. Cl Traces showing the radial component of the electric field, E_r . The traces are computed during a FDTD simulation in the wet model. The trace locations are within the borehole (black dots in Figure 8). The vertical lines correspond to the times of the snapshots (Figure 8).

FIG. 11. Attenuation coefficient, phase velocity, and group velocity of the guided wave. These quantities are calculated during a FK simulation for the wet model. Also shown are estimates of the attenuation coefficient, the phase velocity, and the amplitude of the guided wave, all of which are obtained by processing traces from the FDTD simulation (Figure 10).

FIG. 12. (a) Voltage measured in the TX coaxial cable where it attaches to the transmitter in the prototype tool (Figure 1c). This voltage was used in all laboratory tests. Also shown is an analytical approximation to the measured voltage, which is used in the FDTD simulations. (b) Frequency spectra of the measured voltage and the analytical approximation.

FIG. 13. Traces measured during the laboratory tests and traces calculated with FDTD simulations. The traces show the voltages in the RX coaxial cable where it attaches to the receiver.

FIG. A1. Region of the complex plane in which a value for k is sought to satisfy equation A-4. The points indicate where the absolute value of the right-hand-side of equation A-4 is calculated to find a local

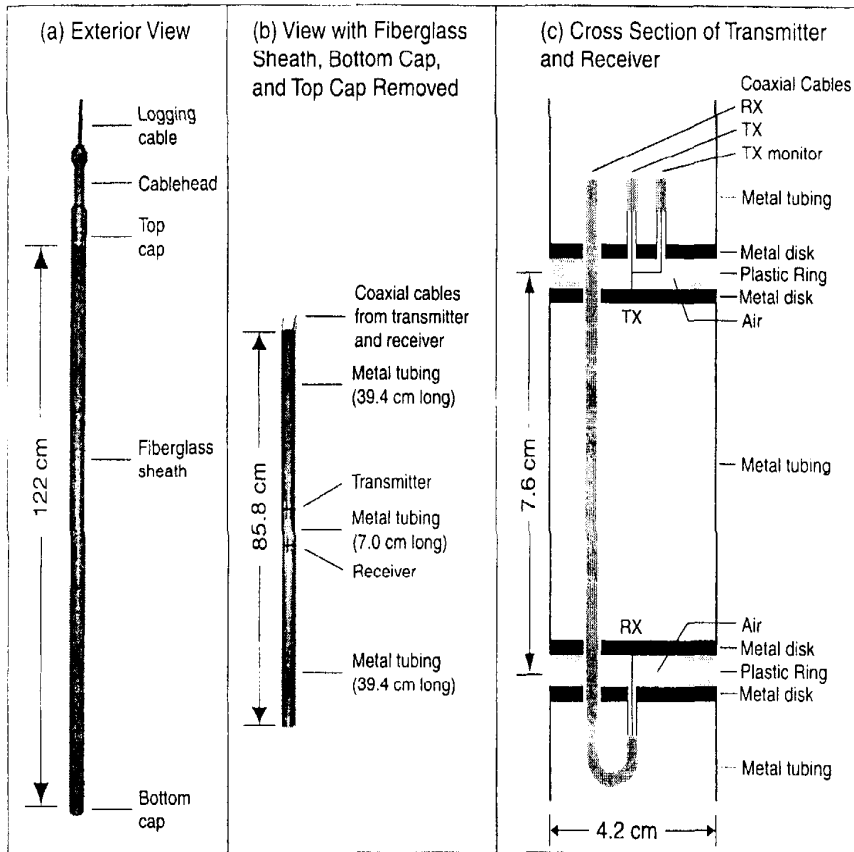


Figure 1
 Ellefsen, Abraham, Wright, Mazzella
 Numerical Study of Electromagnetic Waves
 Generated by a
 Prototype, Dielectric Logging Tool

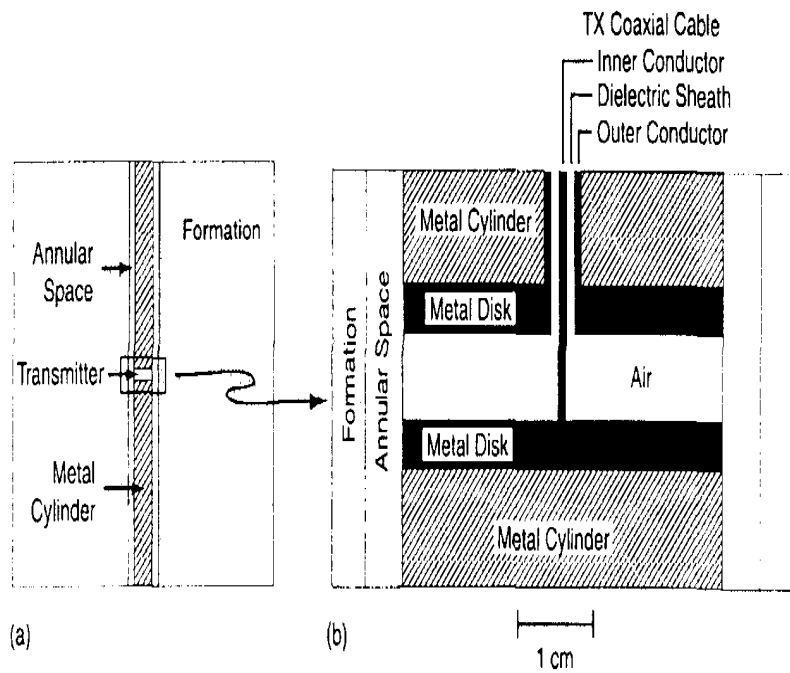


Figure 2
 Ellefsen, Abraham, Wright, Mazzella
 Numerical Study of Electromagnetic
 Waves Generated by a
 Prototype, Dielectric Logging Tool

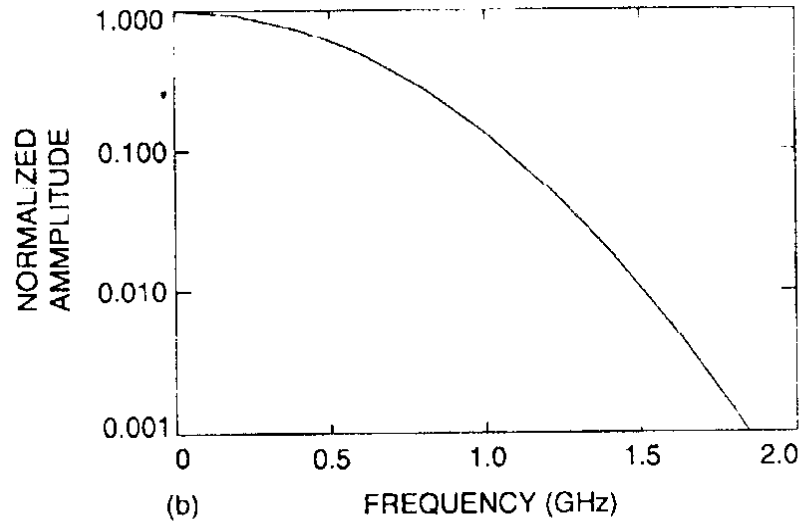
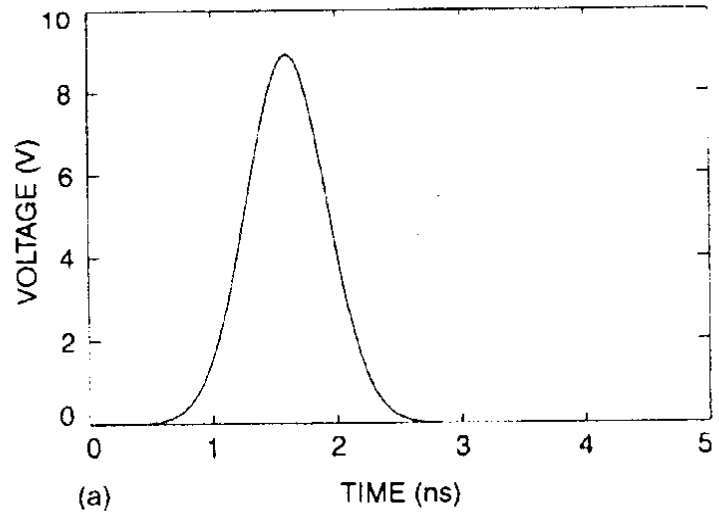


Figure 3
Ellefsen, Abraham. Wright, Mazzella
Numerical Study of Electromagnetic
Waves Generated by a
Prototype, Dielectric Logging Tool

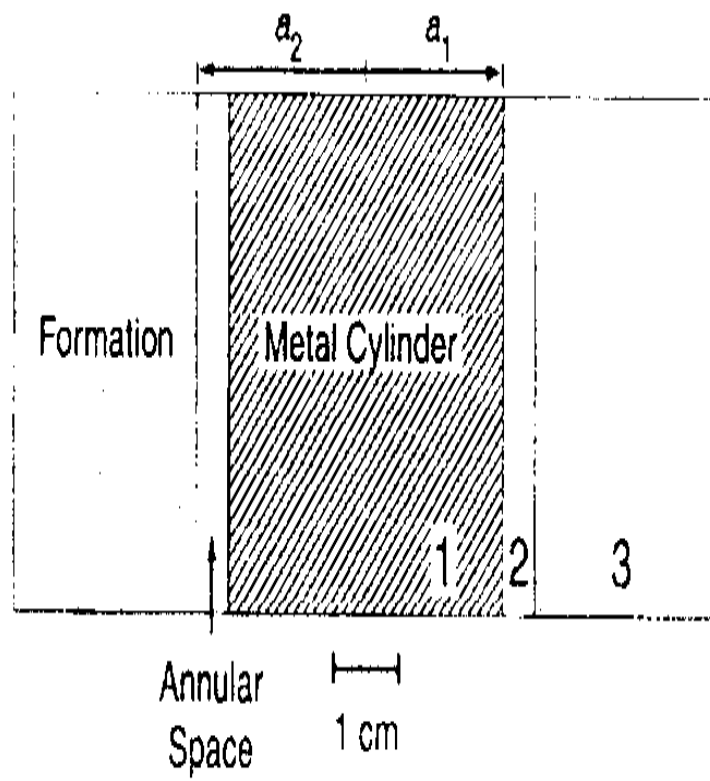
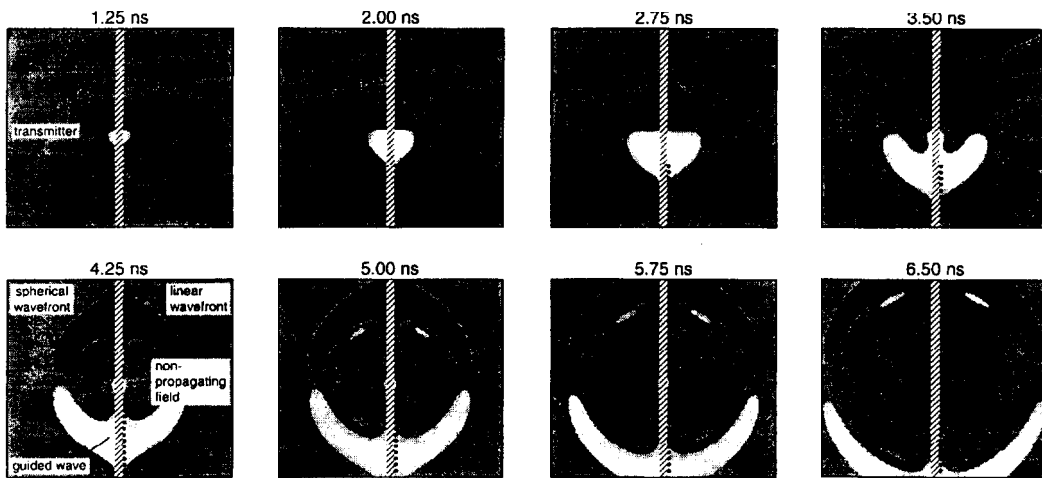


Figure 4
Ellefsen, Abraham, Wright, Mazzella
Numerical Study of Electromagnetic
Waves Generated by a
Prototype, Dielectric Logging Tool



Explanation

1. The snapshots show the radial component of the electric field, E_r .
2. The width and the height of each image correspond to 1.8 and 1.6 m, respectively. Because of this scale, the fields within the transmitter and borehole are difficult to observe.

Metal cylinder in the model tool (Figure 2)
 Approximate location of trace (Figure 6)

Figure 5
 Ellefsen, Abraham, Wright, Mazzella
 Numerical Study of Electromagnetic
 Waves Generated by a
 Prototype, Dielectric Logging Tool

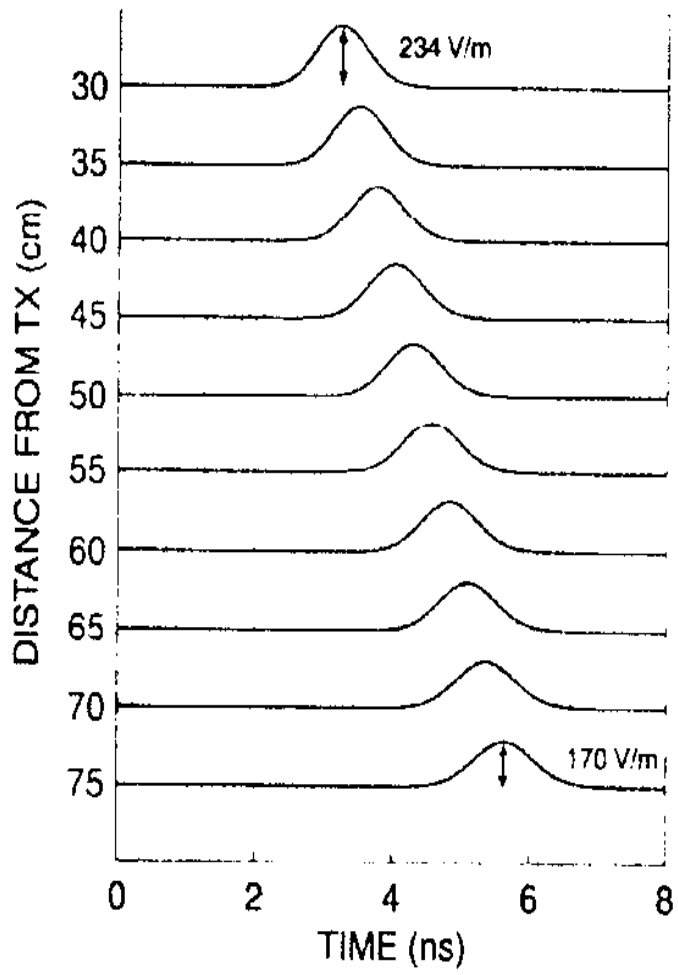
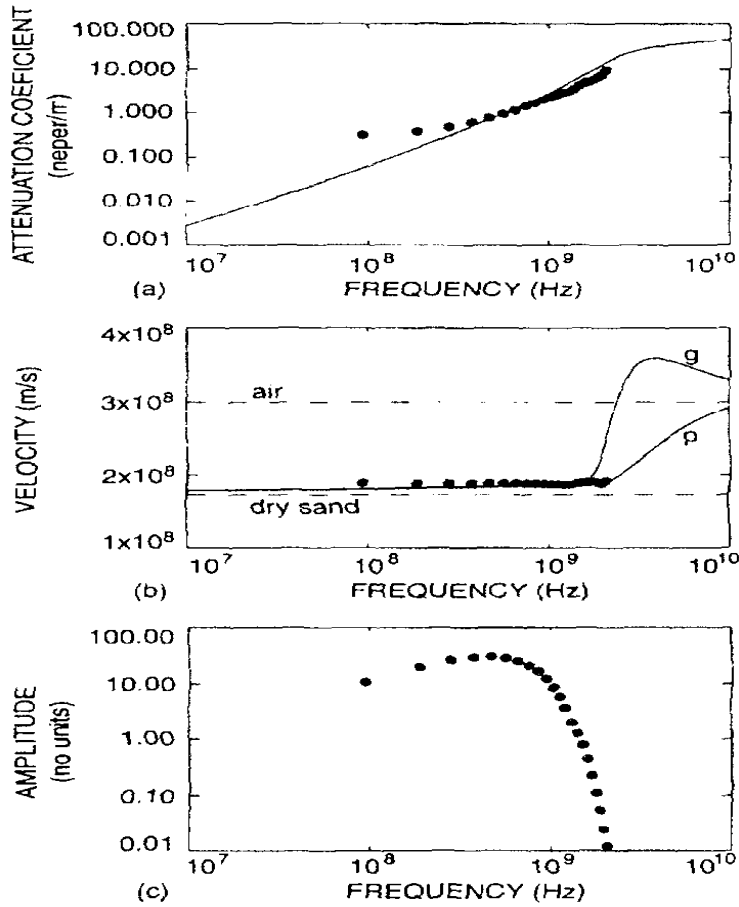


Figure 6
Ellefsen, Abraham, Wright, Mazzella
Numerical Study of Electromagnetic
Waves Generated by a
Prototype, Dielectric Logging Tool



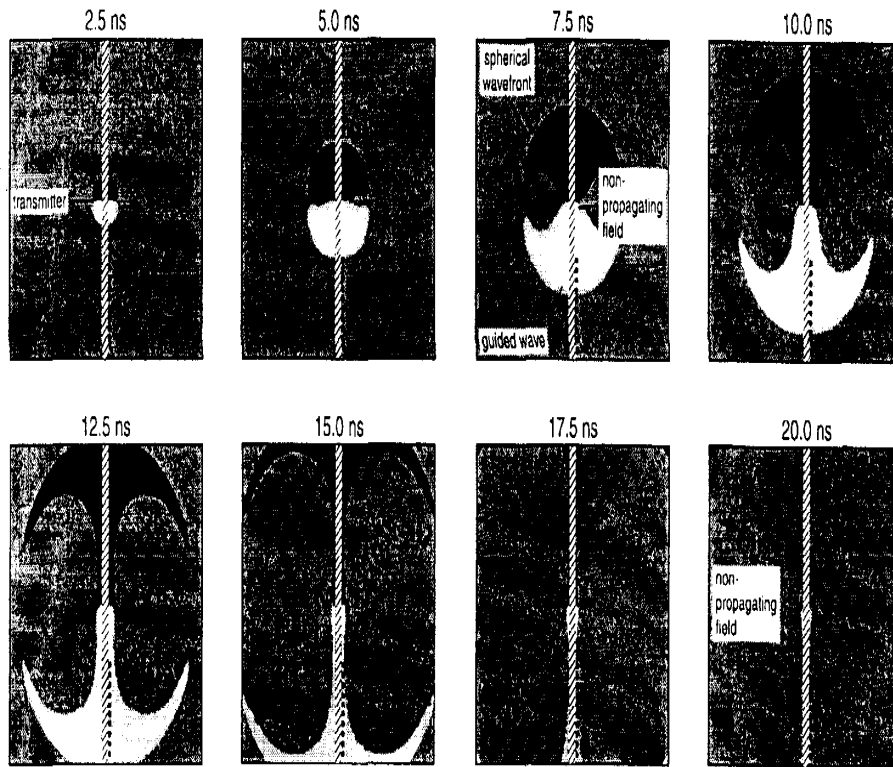
Explanation

— Attenuation coefficient, phase velocity (p), or group velocity (g) calculated during a FK simulation

••••• Amplitude estimated from the traces computed during the FDTD simulation

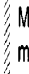
- - - Phase velocity of a plane wave in either air or dry sand


Figure 7
 Ellefsen, Abraham, Wright, Mazzella
 Numerical Study of Electromagnetic
 Waves Generated by a
 Prototype, Dielectric Logging Tool



Explanation

- The snapshots show the radial component of the electric field, E_r .
- The width and the height of each image correspond to 1.8 and 1.6 m, respectively. Because of this scale, the fields within the transmitter and borehole are difficult to observe.

 Metal cylinder in the model tool (Figure 2)

 Approximate location of trace (Figure 10)

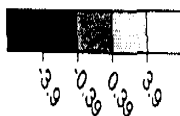
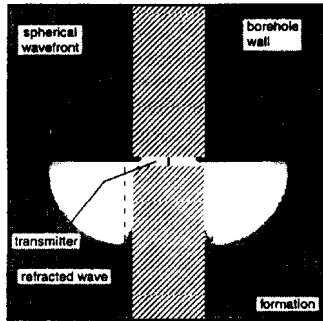


Figure 8
 Ellefsen, Abraham, Wright, Mazzella
 Numerical Study of Electromagnetic
 Waves Generated by a
 Prototype, Dielectric Logging Tool



Explanation

1. The snapshot shows the radial component of the electric field, E_r , at 0.8 ns.
2. Both the width and the height of the image correspond to 0.19 m.

Metal cylinder in the model tool (Figure 2)

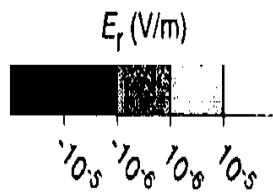


Figure 9
 Ellefsen, Abraham, Wright, Mazzella
 Numerical Study of Electromagnetic Waves
 Generated by a
 Prototype, Dielectric Logging Tool

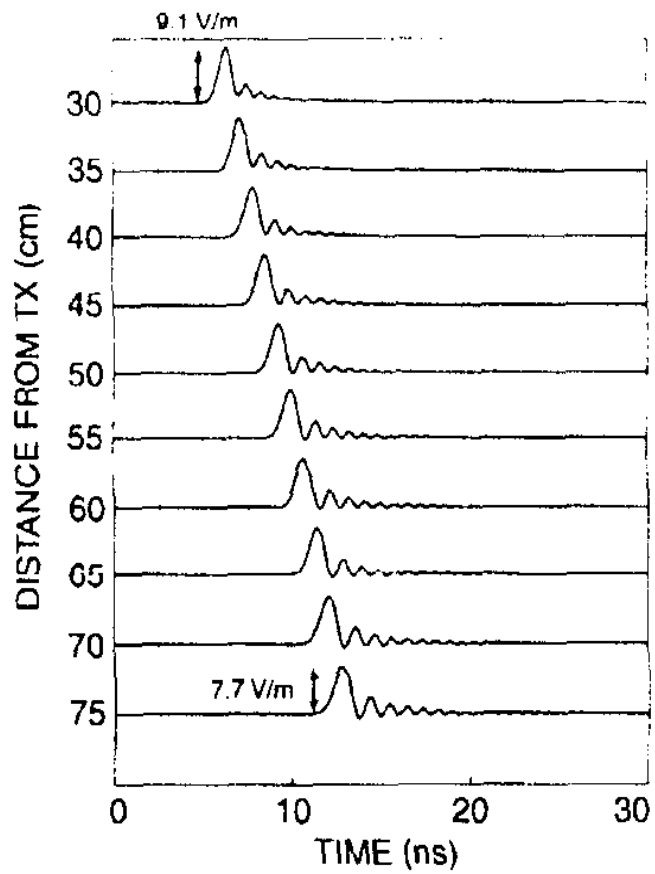


Figure 10
Ellefsen, Abraham, Wright, Mazzella
Numerical Study of Electromagnetic
Waves Generated by a
Prototype, Dielectric Logging Tool

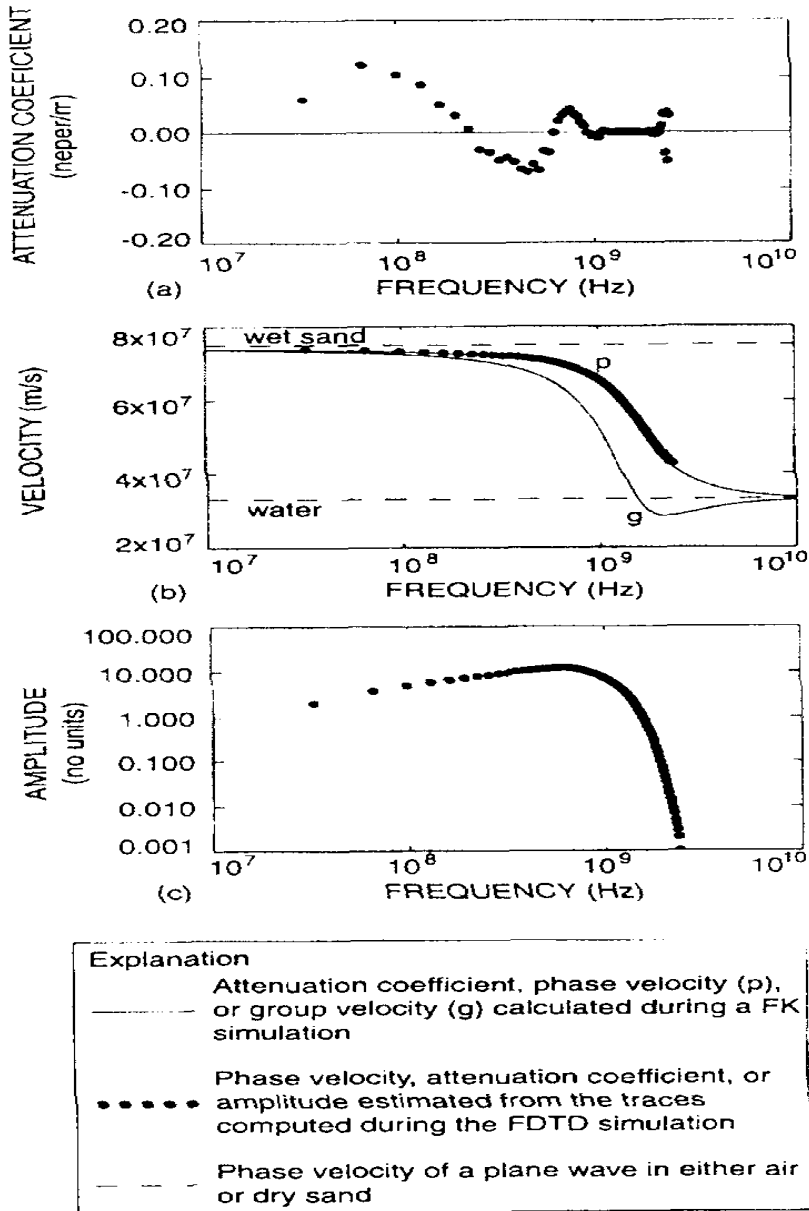
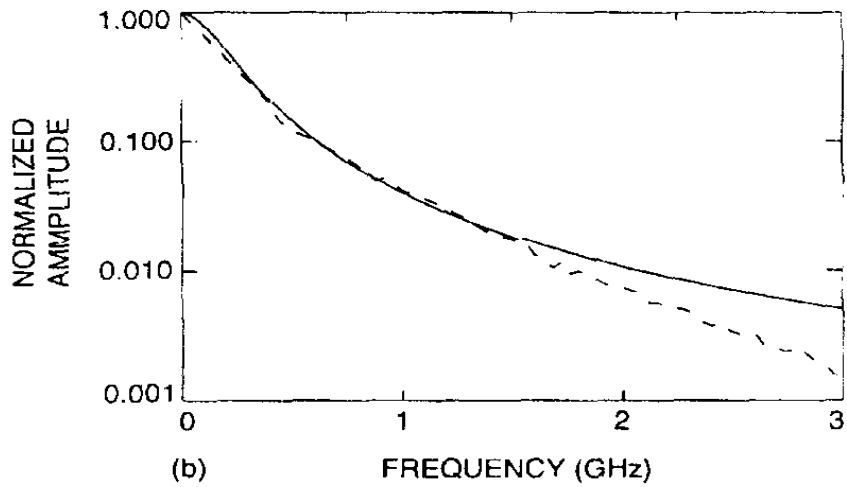
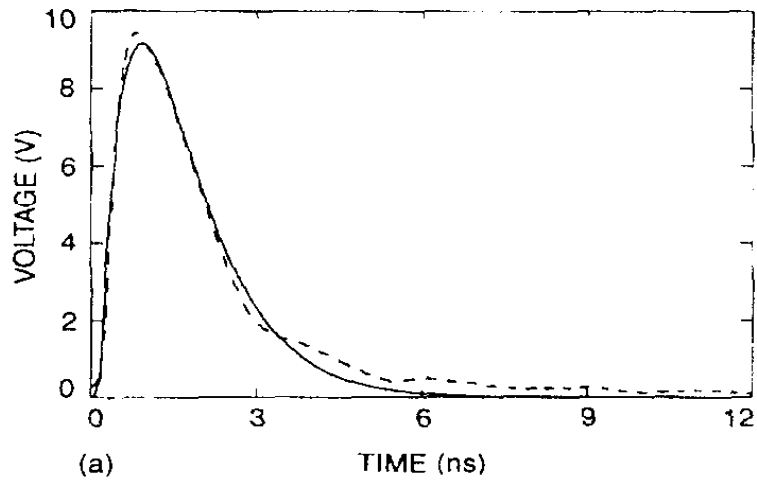


Figure 11
 Ellefsen, Abraham, Wright, Mazzella
 Numerical Study of Electromagnetic
 Waves Generated by a
 Prototype, Dielectric Logging Tool



---	Measured	—	Analytical Approximation
-----	----------	---	--------------------------

Figure 12
 Ellefsen, Abraham, Wright, Mazzella
 Numerical Study of Electromagnetic Waves
 Generated by a
 Prototype, Dielectric Logging Tool

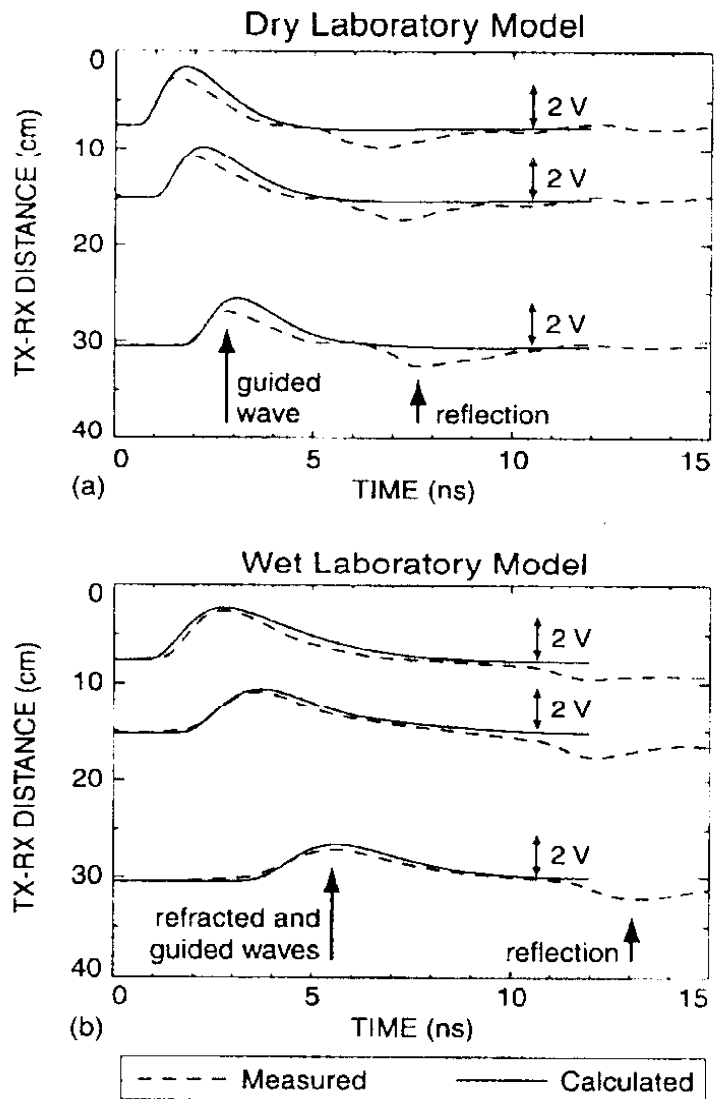


Figure 13
 Ellefsen, Abraham, Wright, Mazzella
 Numerical Study of Electromagnetic Waves
 Generated by a
 Prototype, Dielectric Logging Tool

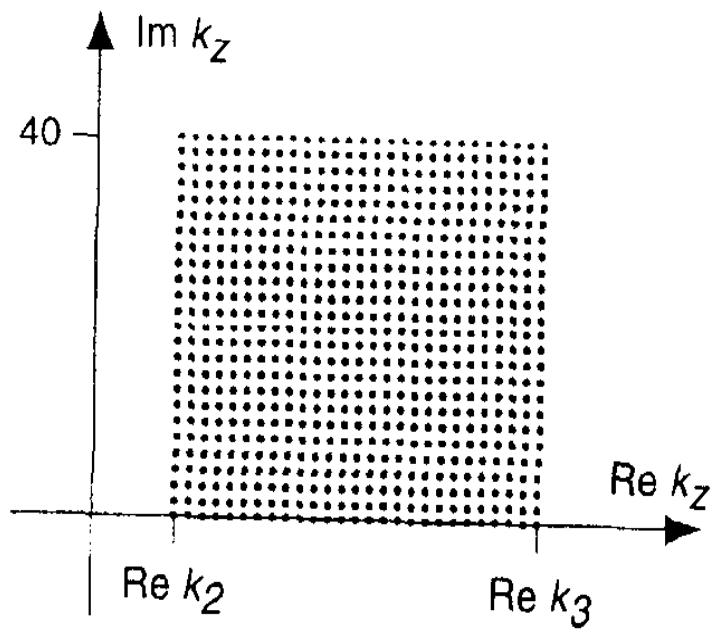


Figure A1
Ellefsen, Abraham, Wright, Mazzella
Numerical Study of Electromagnetic
Waves Generated by a
Prototype, Dielectric Logging Tool